Biosensors and Bioelectronics 168 (2020) 112485

Contents lists available at ScienceDirect

Biosensors and Bioelectronics

journal homepage: http://www.elsevier.com/locate/bios

Electrical Impedance Spectroscopy of plant cells in aqueous biological buffer solutions and their modelling using a unified electrical equivalent circuit over a wide frequency range: 4Hz to 20 GHz

Kian Kadan-Jamal [a,*], Marios Sophocleous [b], Aakash Jog [c], Dayananda Desagani [c], Orian Teig-Sussholz [d], Julius Georgiou [b], Adi Avni [d], Yosi Shacham-Diamand [a,c]

[a] Department of Materials Science and Engineering, Faculty of Engineering, Tel Aviv University, Tel-Aviv 69978, Israel
[b] Department of Electrical & Computer Engineering, EMPHASIS Research Center, University of Cyprus, Nicosia, 1678, Cyprus
[c] Department of Physical Electronics, School of Electrical Engineering, Faculty of Engineering, Tel Aviv University, Tel-Aviv, 69978, Israel
[d] School of Plant Sciences and Food Security, Tel-Aviv University, Tel-Aviv, Israel

ARTICLE INFO

Keywords:
Electrical impedance spectroscopy (EIS)
Plant cells
MSK8
Equivalent circuit

ABSTRACT

A simple, ultra-wide frequency range, equivalent circuit for plant cell suspensions is presented. The model incorporates both the interfacial interactions of the suspension with the electrode, dominant at low frequencies, and the molecule and cell polarization mechanisms dominant at higher frequencies. Such model is useful for plant cell characterization allowing a single set of parameters over >9 orders of magnitude, whilst allows electronic simulations over the whole frequency range using a single model, simplifying the design of electronic systems of integrated plant cell sensors. The model has been experimentally validated in the frequency range of 4 Hz–20 GHz with each component in the circuit representing a physical phenomenon. Various cell concentrations (MSK8 tomato cells in Murashige and Skoog media) have been investigated, showing clear correlations of the cell capacitance increasing within the range of 200–600 pF, whilst cell resistance (R) decreasing within the range of approximately 0.8–3 kΩ within the cell concentration X–Y cells/mL range. This is the first model ever reported that covers such a wide frequency range and includes both interfacial and polarization effects in this simple form.

1. Introduction

The increasing demand for higher qualities and quantities of agricultural products (Carvell and Dowd, 2006; Khaled et al., 2016) has boosted the demand for online, non-destructive monitoring of plants and produce. Monitoring can be achieved at all levels: from plant health, soil chemistry, volatiles, cellular, or sub cellular levels up to actual produce quality. Several techniques are available to monitor the aforementioned parameters, with impedance spectroscopy being probably the most powerful.

Electrical Impedance Spectroscopy (EIS) is widely applied in characterization of insulating, semiconductor, and even conducting materials, such as electrolytes (Corona-Lopez et al., 2019; Guan et al., 2004). The technique uses the materials' dielectric properties that depend on the distribution of electric charges, internal and on their surface, and their interaction with an electric field. These properties depend on material composition and are useful in characterizing composite materials, both organic and inorganic, where the analyte under investigation is distributed in fluid media. The internal and surface charges can be either inherent within the structure (i.e. molecules, organelles, cells etc.) or temporarily induced on their surfaces (Asami, 2002a). Hence, dielectric properties can provide valuable information about various biological analytes, such as a mixture of various molecules (Skierucha et al., 2012) or cell/electrolyte suspension. Impedimetric analyses of cell cultures have been used in the past for non-destructive monitoring of the morphology, viability, and environmental change of cells for many cell types in various media under different conditions (Andreescu et al., 2004; Guan et al., 2004; Guo et al., 2006; Lei et al., 2014; Liu et al., 2009). Several models have been proposed relating the dielectric properties of plants, plant cell cultures, and agricultural products with biophysical and electrical properties of heterogeneous systems at the molecular and macroscopic levels (Asami, 2002b; Asami and Yamaguchi, 1992; Nelson, 1991). There also exist studies reporting the use of EIS for real-time monitoring allowing for better control of cell

* Corresponding author.
E-mail address: kiankadan@mail.tau.ac.il (K. Kadan-Jamal).

https://doi.org/10.1016/j.bios.2020.112485
Received 25 April 2020; Received in revised form 27 July 2020; Accepted 28 July 2020
Available online 19 August 2020

culturing with higher yields (Chen et al., 2005; Guo et al., 2006; Lei et al., 2014; Liu et al., 2009; Ribaut et al., 2009). Typically, EIS has been used to assess the dielectric properties of biological units in an ionic conducting medium (Grimnes et al., 2015), e.g. aqueous cell suspension, biological fluids, aqueous assays etc (Bera et al., 2016). EIS measurements provide information that is represented either by an effective complex dielectric constant or by an equivalent lumped electrical circuit that includes capacitive, conductive/resistive, and inductive components. These components represent the various mechanisms affecting the overall electric and dielectric properties of the sample and the electrodes together with the interconnects used, over a defined range of frequencies.

Biological samples, almost always, either have a certain degree of water content or are in an aqueous buffer solution. Water has a strong interaction with the electric field at microwave frequencies due to its dipolar nature and due to dispersion associated with its dielectric properties (Trabelsi and Nelson, 2003). Therefore, as the medium's dielectric properties can be significantly affected by cell properties and cell concentrations, especially in aqueous media, the moisture content and bulk density of cells can be monitored using EIS techniques (Nelson, 1981; Trabelsi and Nelson, 2016). EIS investigations of biological electrolytes, available in the literature, usually cover a relatively limited frequency range depending on the equipment and setup. There is a significant amount of data published regarding the lower end of the spectrum – up to a few MHz, and some data at frequencies higher than 1 GHz. This is probably due to the complexity, the level of expertise needed at high frequency measurements, and also the high cost of equipment for radio and microwave frequency EIS systems (Asami et al., 1996). On the other hand, there are relatively simple, low-cost, and user-friendly electronic instruments, such as potentiostats with an EIS option, for the lower frequency range, up to ~100 kHz-1 MHz. Nevertheless, there are a few reported cases yielding data on cell suspensions at high frequencies (Beving et al., 1994; Carvell and Dowd, 2006; Irimajiri et al., 1978; Markx and Davey, 1999; Surowiect et al., 1986). They show that EIS may provide important information related to the cells, i.e. shape, membrane properties, cytoplasm, cell surface, nuclear envelope, intracellular phases, etc.

The first investigation of dielectric properties of biological cells was performed more than a century ago (Höber, 1910), in which the cells were characterized as a poorly conducting membrane enclosing a conducting and polar cytoplasm. The efficiency and effectiveness of the impedimetric and dielectric methods (Asami et al., 1980), are in the evaluation of passive electrical properties (Pethig and Kell, 1987) of cell membranes (Herman P. Schwan and Shiro Takashim, 1991) is based on the reality that the presence of the cell membrane - low-conductivity layer separating two different high-conductivity media (the cytosol and the extracellular medium) gives rise to a marked conductivity dispersion (Markx and Davey, 1999) in the radio wave frequency range (Bordi et al., 1993). The general tendency is for permittivity to fall, and conductivity to concomitantly increase, in a series of steps as frequency increases. These step changes are called dispersions (Markx and Davey, 1999) and each one reflects the loss of a particular polarization process at increasing frequencies. Biological materials can show quite large dispersions, especially at low frequencies (Asami, 2014; Asami and Yamaguchi, 1992). For practical applications in agrophysics, the applied frequencies usually do not exceed 20 GHz (Skierucha et al., 2012). Both the medium and the cells affect the overall electrical properties of a suspension placed between the electrodes of an EIS setup. In a dilute system (with respect to cell density), the resistance will, for example, be governed by electrolytes and especially salt concentrations in the liquid. The capacitance or ability to at least temporarily store electrical energy by charge separation, however, will exist mainly across cell membranes of living organisms (T. Hanai, K. Asami et al., 1976). This hypothesis has been verified in various scientific studies dealing with diversification of the quality parameters based on dielectric properties of several types of tested cells, e.g. yeast, liver cells, lymphoblast, *E. coli* bacteria, etc (Asami et al., 1989, 1976; Beving et al., 1994; Bordi et al., 1993; Carstensen, 1967; Irimajiri et al., 1978; Jenin and Schwan, 1980; Schwan and Li, 1953; Surowiect et al., 1986; Touw et al., 1973). There is a variety of published research, focused on the impedimetric properties of biological cell culture (i.e. yeast (Chen et al., 2005), human hepatocarcinoma cells (Guo et al., 2006), human oral cancer cells (OEC-M1) (Lei et al., 2014), human oesophageal cancer cell lines (KYSE30) (Liu et al., 2009), red blood cells (RBC) (Ribaut et al., 2009), etc.) but there are few on plant cell cultures using EIS/Impedimetric analysis (Asami and Yamaguchi, 1992; Bera et al., 2016).

The potential to monitor cell concentration, cell size, metabolic state, cell morphology, apoptosis, immobilization, viral infection, and virus release as well as several other parameters in real-time, enables improved process control and understanding of the complex mechanisms during several processes. The potential of EIS, may well reach beyond measuring viable cell density to more intricate issues, such as the physiological state of the cell or organism. In comparison to other common methods, EIS allows for non-invasive and non-destructive, online process monitoring and control for suspension cultures and even cells attached to solid carriers (Carvell and Dowd, 2006), as probes can be sterilized in-situ and are available as disposable units (Markx and Davey, 1999). However, practical implementation of material characterization in a broad frequency range using dielectric spectroscopy is still rare, and more research and development is needed to assess the practicality of such techniques at these ranges.

It is clear that there is a need for more data and models linking the information about the dielectric properties of biological materials from low, medium, and high frequency ranges. Although a variety of equivalent circuits for animal cell suspensions exist, plant cell has different morphology and some unique features such as cell walls and use different buffer solutions compared to animal cells. This leads to different characteristic frequencies and values in the dispersion curved hence, plant cells required different modelling approach when compared to animal cells. This need is highlighted by the current trend in electronics to increase the use of Radio Frequency Integrated Circuits (RFIC) following the need for wider bandwidth information and communication technologies. RFIC technology is creating an opportunity to have, in the near future, lower cost, high quality, field-deployable, reliable and inexpensive ultra-wideband EIS components and systems for the fields of medicine, food, agriculture and environmental monitoring. However, this will only be feasible if the EIS sensor can provide a reproducible signal, with good signal to noise ratio and low error rate (both false positive and false negative). The signal mentioned above can be understood as the change in one of the impedance components and its assessment from the testing results, which also depends on the electrical modelling of the system under test. In order to design and successfully manufacture EIS systems that can span through the low frequency range (few Hz down to μHz) up to tenths of GHz, a reliable model of the cell suspension is required. Currently, engineers and scientists use discrete models for the low frequency (Randles model) and several other models for the high frequency (>1 GHz) leaving a significant frequency range usually uncovered.

Therefore, a model that can combine the low frequency range with the high frequency range and be accurate even for the mid-frequency range will have a major impact to the design of the electronic equipment required for EIS measurements within any frequency range.

This paper presents a systematic approach to generate a unified equivalent circuit representation, for the assessment of the impedimetric properties of plant cells (tomatoes MSK8) in aqueous biological growth media Murashige and Skoog (Murasnige and Skoog, n.d.) (MS) and in an ultra-wideband frequency range (4 Hz-20 GHz). The model was conceived taking into consideration both electrode and bulk effects. This information depends on relationships between the circuit components, the cell concentrations, the cell types, and the media. Using equivalent circuits is a relatively simple tool that is compatible with common electrical engineering Computer Aided Design (CAD) tools; therefore, it can be used for future biosensor design and integration with very low-cost, conventional electronic systems. Having single model will benefit both circuit simulations for electronic circuits characterizing or incorporating cells and also plant research allowing a simple set of parameters over >9 orders of magnitude.

2. Materials and methods

2.1. Preparation and analysis of cells

2.1.1. Cell cultures

Tomato (*S. lycopersicum* cv Mill.; line MSK8 (Koornneef et al., 1987)) cell suspension cultures were grown in Murashige and Skoog (MS) (Murasnige and Skoog, n.d.) medium including vitamins (Duchefa Biochemie), supplemented with 30 g/L sucrose, 1 mg/L 2,4-dichlorophenoxyacetic acid (2,4-D) and 0.1 mg/L kinetin, which was set to pH 5.7. The cell culture was centrifuged at 25 °C in the dark, at approximately 100 rpm. Sub-culturing was performed every 2 weeks. MSK8 cells were used 14–20 days after sub-culturing and were diluted before the experiment in fresh MS medium.

2.1.2. TEM analysis

Cells were precipitated from the MS and washed several times in PBS buffer and then stored in 2.5% Glutaraldehyde in PBS over night at 4 °C followed by incubation at 1% OsO_4 in PBS for 2 h at 4 °C. Dehydration was carried out in graded ethanol followed by embedding in Glycid ether. Thin sections were mounted on Formvar/Carbon coated grids, stained with uranyl acetate and lead citrate and examined in Jeol 1400 – Plus transmission electron microscope (Jeol Inc., Japan). Example for the TEM analysis is shown in Supplementary Material (Section S1).

2.2. EIS measurements

EIS measurements were carried out for a frequency range of 4 Hz–20 GHz using multiple instruments. Three different probes were used to run the experiments for the low frequency range (4 Hz–5 MHz), the mid-frequency range (100 kHz–3 GHz), and the high frequency range (200 MHz–20 GHz). The measurement ranges relate also to the cell line sample, which had characteristic dispersions at those ranges. For all the experiments, cells at specific concentrations were filtered out from the growth medium and then suspended again in a fresh medium (total volume of approximately 700 μL) before the beginning of each measurement. All measurements were performed at room temperature (25 °C).

The experiments for each cell concentration have been repeated 3–5 times with the difference in the obtained data to be well within the error margins of the equipment used. More details about the equipment used and their error margins can be found in the Supplementary Material and the equivalent MethodsX paper.

Table 1
The equivalent circuit components expressed in terms of the Debye model components. Note that we assume RC = τ.

Type	Nomenclature	Expression
Capacitance (F)	C_1	$C_1 = \varepsilon_0 \varepsilon_{r,\infty} \cdot \frac{A}{d}$
	C	$C = \varepsilon_0 [\varepsilon_{r,0} - \varepsilon_{r,\infty}] \cdot \frac{A}{d}$
Resistance (Ω)	R	$\frac{1}{R} = \sigma_r \cdot \frac{A}{d} = \frac{C}{\tau}$
	R_1	$\frac{1}{R_1} = \frac{1}{G_1} = \frac{\sigma}{\varepsilon_0} \cdot \frac{A}{d}$

3. Electrical modelling

Electrical Impedance Spectroscopy (EIS) is a common method used for the characterization of dielectric materials in general and biological materials and solutions in particular. The theory is well established and in this work we follow a common formulation mentioned in various textbooks (Barsoukov, Evgenij, 2005; Orazem, M. E., & Tribollet, 2017). Here, we focus on cell-line suspensions containing buffered electrolyte and cells. Although it is called "impedance spectroscopy" and the results can be presented as the impedance versus frequency, it is very common to present the results in the form of admittance, S parameters, and/or dielectric constant versus frequency. Another way to represent the data is using an equivalent electrical circuit. Each component, or a group of components, represents some physical mechanism, which is more dominant or noticeable in a specific frequency range. In this paper, we demonstrate a unified equivalent circuit, based on known models (i.e. Orazem M (Orazem, M. E., & Tribollet, 2017). and Barsoukov, Evgenij, and J. Ross MacDonald (Barsoukov, Evgenij, 2005)) combining all the dominant effects. The advantage of having one model is twofold:

1. It allows for simulation of the system, where the biological solution is embedded in an electronic system. It can be done using computer aided design (CAD) tools like SPICE, which is a standard tool among circuit designers.
2. A simple representation can be achieved over almost 10 orders of magnitude providing more information on the analyte characteristics; e.g. better sensing or screening.

The approach presented here in modelling the impedance of biological samples is by using two different equivalent circuits, each one representing the behavior of a system in a different frequency range, thus creating networks for each frequency regimes while forming a total equivalent circuit composed of the serial combination of those networks.

At low frequencies, the impedance is dominated by the electrolyte/electrode interface. Hence, the Randles model (Randles, 1947) is used for that regime. In the medium and high frequency range, the impedance is dominated by the electrolyte impedance, the solution conductivity, and various loss mechanisms due to the presence of cells in the electrolyte. Stitching the two models together is relatively simple to execute since in the medium frequency range, the solution impedance, which is common to the two models, is dominant. In the Randles model, the serial resistance is the dominant part. In the high frequency model, where

Debye's representation of the impedance was used, this electrolyte conductance is represented in parallel to the other components that represent other loss mechanisms in the electrolyte. There is a slight inaccuracy in this assumption, since the serial resistance in the Randles model includes also contact and wire resistance; however, in the apparatus used, those other parasitic components are much smaller compared to the electrolyte impedance, which is due to its ionic conductivity.

3.1. Medium to high frequency range

In the medium to high frequency range (>10 MHz), most publications present the impedance data using the complex dielectric constant as the figure of merit, representing both the dissipating and non-dissipating components of the material. In this section, we follow standard equivalent circuit models that appear in the literature (Barsoukov, Evgenij, 2005; Orazem, M. E., & Tribollet, 2017). The equivalent circuit model was adapted according the experimental setup.

The dielectric constant is usually represented as a function of the frequency, for small signal excitation and it includes both real and imaginary parts:

$$\varepsilon(\omega) = \varepsilon^{'}(\omega) - j\varepsilon^{''}(\omega) \tag{1}$$

The dielectric constant can be extracted from the measured impedance, admittance, or S-parameters using proper modelling. There are few ways to model the dielectric constant: the Debye model (P. Debye, 1929), the Cole-Cole model (Cole and Cole, 1942), the Davidson-Cole model (Davidson and Cole, 1950) and the Havriliak-Negami model (Havriliak and Havriliak, 1996; Havriliak and Negami, 1966). In this paper, we will follow the Debye model since it yields, as will be shown later, a rather simple lumped equivalent circuit.

The Debye model for the relative dielectric constant $\varepsilon_r(\omega)$ of the biological solution is defined as:

$$\varepsilon_r(\omega) = \varepsilon_{r,\infty} + \frac{\varepsilon_{r,0} - \varepsilon_{r,\infty}}{1 + j\omega\tau} + \frac{\sigma}{j\omega\varepsilon_0} \tag{2}$$

Where ε_0 is the dielectric constant of vacuum (8.854×10^{-12} C/V m), $\varepsilon_{r,\infty}$ is the relative dielectric constant at very high frequency, $\varepsilon_{r,0}$ is the relative dielectric constant at low frequency, ω is the angular frequency (rad/s), and σ is the specific conductivity of the electrolyte (S/m). In this model, we combined the classical Debye model with the solution conductivity model in a way that the impedances representing those effects will be in parallel to each other. That complex dielectric constant (Eq. (2)) is used to calculate the admittance Y(ω) of an equivalent capacitor C* with an area A (m^2) and distance d (m) between the plates:

$$Y(\omega) = j\omega C^{*} = j\omega\varepsilon_0 \cdot \frac{A}{d} \cdot \left[\varepsilon_{r,\infty} + \frac{\varepsilon_{r,0} - \varepsilon_{r,\infty}}{1 + (\omega\tau)^2}\right] + \left[\sigma_r \cdot \frac{(\omega\tau)^2}{1 + (\omega\tau)^2} + \sigma\right] \cdot \frac{A}{d} \tag{3}$$

Where: $\sigma_r = \frac{\varepsilon_{0r,0} - \varepsilon_{r,\infty}}{\tau}$.

Observing this admittance, Y(ω), the real part can be interpreted as a resistive component and the imaginary part can be interpreted as a capacitive component. However, these components depend on the frequency. Therefore, further simplification of the model, to frequency-independent components is required in order to allow for a simple RC network representation. This has been accomplished following the observation that the network that is shown in (Supplement Fig. S3), has the same frequency functional dependence for its admittance as that written in the admittance derived from the Debye model (Eq. (3)):

$$Y = j\omega\left[C_1 + \frac{C}{1 + (\omega RC)^2}\right] + \frac{1}{R} \cdot \frac{(\omega RC)^2}{1 + (\omega RC)^2} + G_1 \tag{4}$$

This model includes three circuits in parallel: a capacitor, a resistor, and a resistor in series with a capacitor.

Comparing expressions 3 and 4, we can show that the components of the admittance equivalent circuit (Supplement S3) can be written as function of the Debye model components as in Table 1.

In the case where there are a few loss mechanisms in the solution, in addition to that of the electrolyte, we can assume that each one of them contributes a single time constant to the effective dielectric constant. Therefore, the effect of the loss mechanism can be modelled as an additional RC element as shown in Fig. 1.

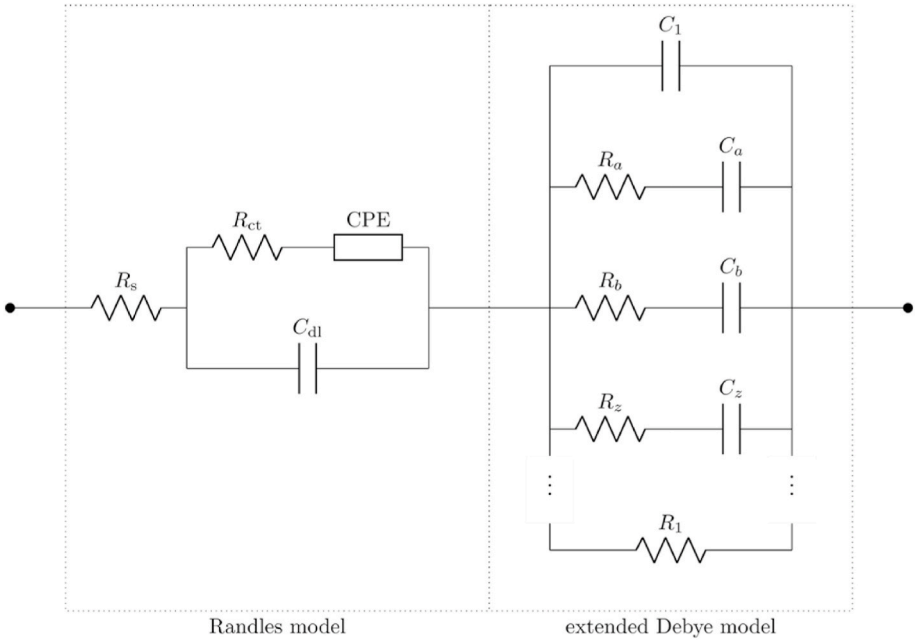

Fig. 1. The unified equivalent circuit model of the cell-line suspension, and in the extended Debye model section, the equivalent circuit in the case when there are a few dissipative components. R_a, R_b …, R_z are the equivalent resistors. C_a, C_b …, C_z are the equivalent capacitors (Barsoukov, Evgenij, 2005).

3.2. Unified model

A unified model is presented here that can be used to characterize suspensions in a frequency range spanning ten orders of magnitude (Fig. 2). This model includes both the Randles model and the model presented in the previous section. The Randles model is well described in the literature (Randles, 1947). At low frequencies, typically below 1 kHz, the impedance of the double layer capacitance, C_{dl}, becomes of the same order of magnitude as the series resistance, R_s. In that frequency range, transport phenomena near the electrodes are also observed and are typically modelled by the Warburg impedance, Z_W, or in a more general model as a Constant Phase Element (CPE) in series with the charge transfer resistance, R_{ct}. For more details on the Randles model and how each component is represented please refer to Bard and Faulkner (2001). The Randles model is sufficient up to frequencies of less than 10 MHz where the Debye model starts to dominate. Based on the equivalent circuit of the Debye model presented above, C_1 is related to the water polarization whilst C represents the capacitance of due to the presence of the cells. R serves as the resistance of the cells and R_1 the resistance of the solution. The proposed unified model consists of the Randles cell and the Debye-based model in a serial connection. There are two reasons why a serial connection is preferred. First, the two components of the model represent two processes that occur where the total potential over the cell is the sum of the potentials of those components (plus a constant arising from the electrode electrochemical potential). In that case, where the current is the same but the total voltage is the sum, a serial connection is preferred. Second reason is that in a serial connection, the higher impedance dominates and this is what it is observed from the experiments.

Note that on the frequency range, the model is degenerated into a single resistor with a value that depends on the frequency:

1. At very low frequencies, the impedance would be equal to $R_s + R_{ct} + CPE + R_1$
2. At medium frequencies, where the Cdl short-circuits the other branch of the Randle model, the impedance would be $R_s + R_1$
3. At higher frequencies, where C short-circuits the Debye model, the impedance becomes $R_s + R_1||R$.
4. At very high frequencies, where C_1 short-circuits the Debye model, the impedance become R_s.

For the apparatus used, the resistance of the electrolyte solution is larger than the other serial resistance components. Therefore, it was assumed that the serial resistance calculated at low frequencies and the parallel resistance measured at high frequency are approximately equal to R_1 at the low side of the medium frequency range or $R_1||R$ at higher frequencies.

4. Results and discussion

4.1. EIS characterization/EIS spectra of the cells

EIS investigation was performed on MSK8 cell suspensions in MS with different cell concentrations of 25%, 50%, 75%, and 100%. The investigation was conducted using three different probes as described in section 2.3. The impedance spectrum is evaluated by fitting the appropriate equivalent circuit parameters to the experimental data. Each element of the circuit contributes predominantly to different frequency regimes, which allows for separation of the effects of the different components of the electrical interface.

The results from each frequency range were fitted separately since different probes were used. More specifically, for the low frequency range, the fitting was achieved by modelling the probe used as a simple inductor with a mean relative error of 5.6–6.7% of the complex impedance. However, for the mid frequency range, the modelling of the probes was much more complicated. Since the probe used was a coaxial airline probe, it was modelled using the simplest transmission line model with an extra resistor and capacitor in parallel (Supplementary Materials Fig. S4).

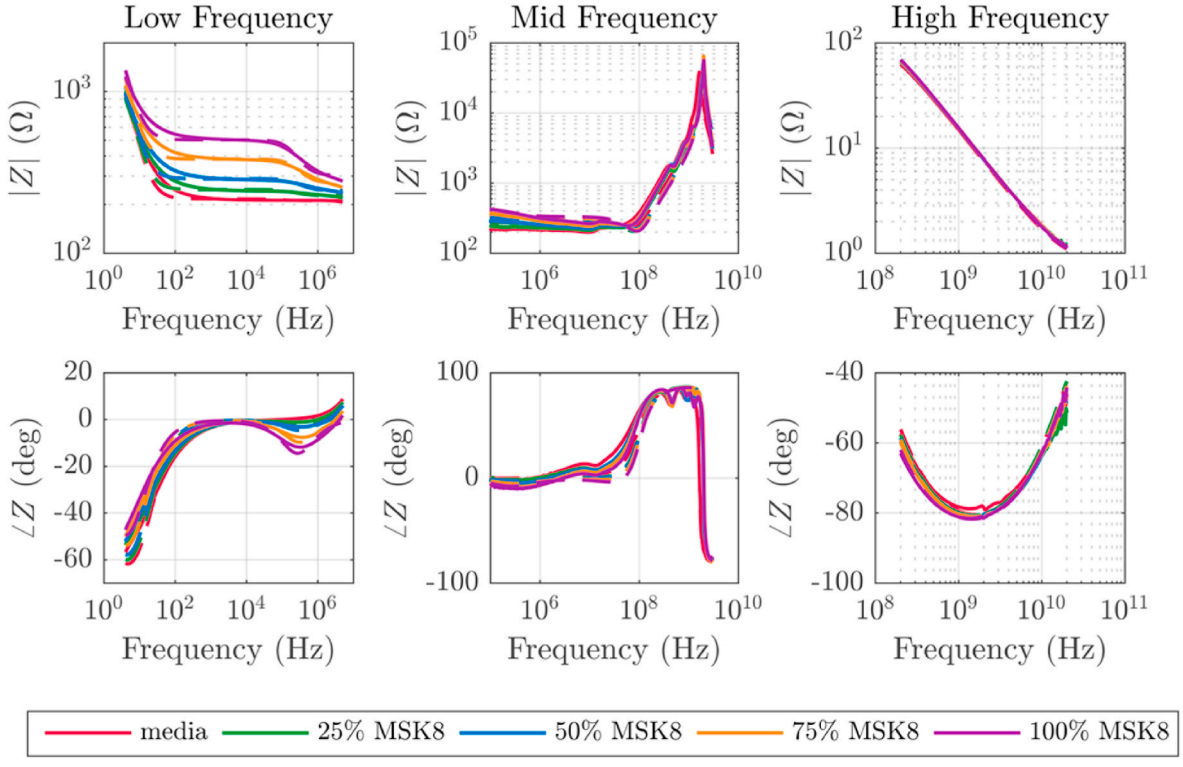

Fig. 2. Impedance magnitude |Z| (Upper) and phase (lower) plots vs. frequency for MSK8 in MS for different concentrations of cells.

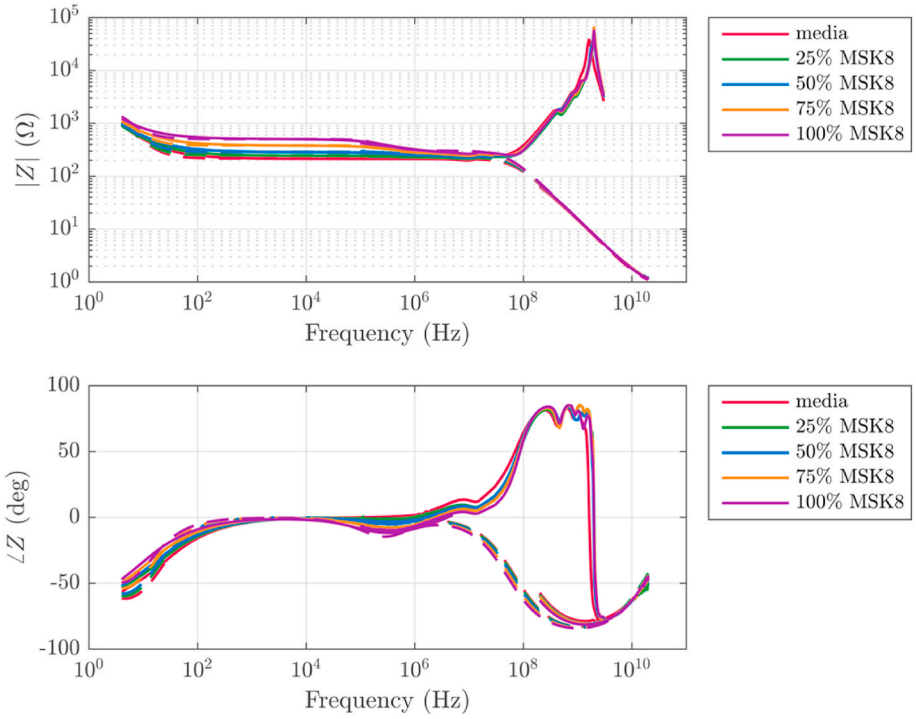

Fig. 3. Merged data after factoring (solid lines) and fitted results (dotted lines) after removal of parasitics.

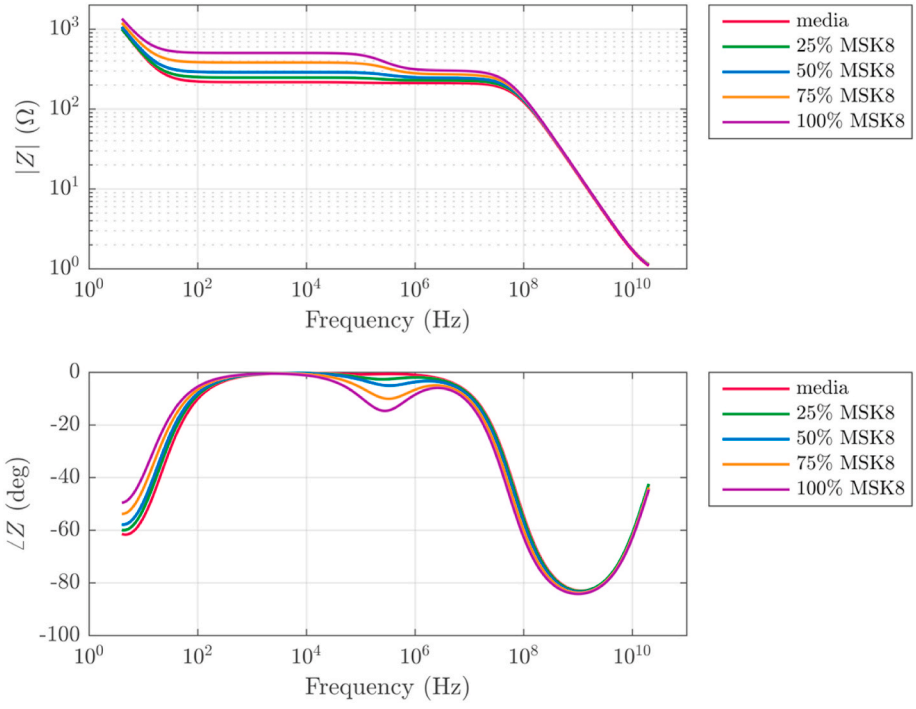

Fig. 4. The simulated behavior of the equivalent circuit with component values obtained by fitting the model to the real data.

This fitting was not as good as the one for the low frequencies and the mean relative error was in the range of 24–30%. Although the error is high, it is because of the multiple time constants that contribute to the peaks observed but for simplicity reasons, the probe was modelled using a single inductor and capacitor for the leads. A more precise model will involve an infinite number of inductors and capacitors, but the complexity of the circuit increases significantly, which defeats the purpose of the model. For the high frequency range, a commercial open-ended probe was used, and the algorithms used to eliminate the effect of the probe were provided by the manufactured and implemented during the probe's calibration, as described in the manual. It is important to note that the output of the algorithms was relative permittivity using the Debye model, which was converted to impedance assuming a complex capacitor. The fitting of the unified model to the high frequency data showed a mean relative error of 1–4% of the complex impedance.

Fig. 3 shows as solid lines, the obtained data of the cells in the MS

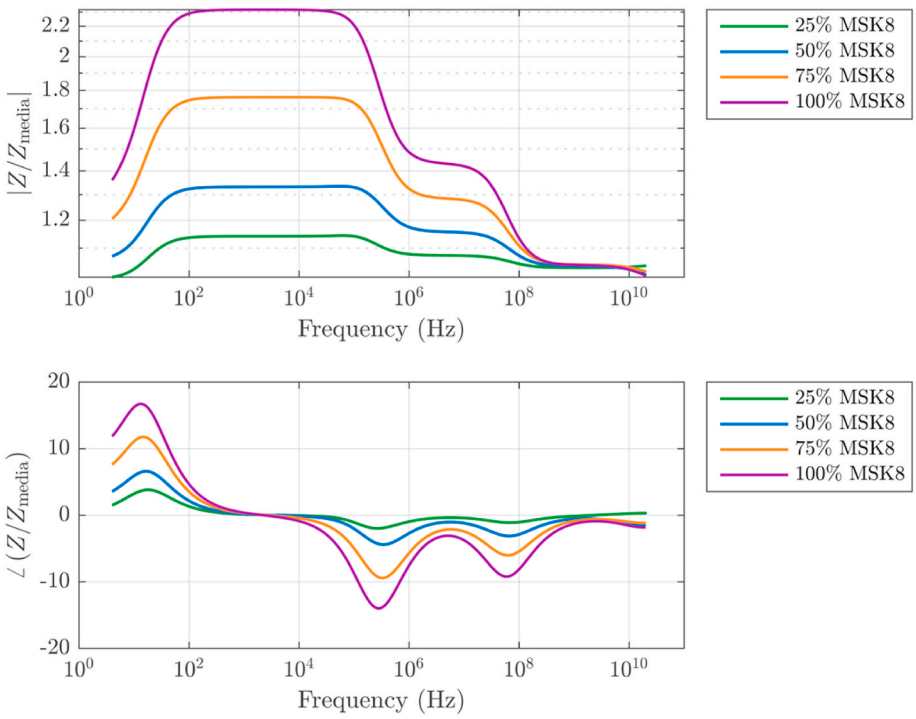

Fig. 5. The normalized data at the full range of frequency (4Hz-20GHz) of the impedance magnitude |Z| and phase vs. frequency for MSK8 in MS for different concentrations of cells.

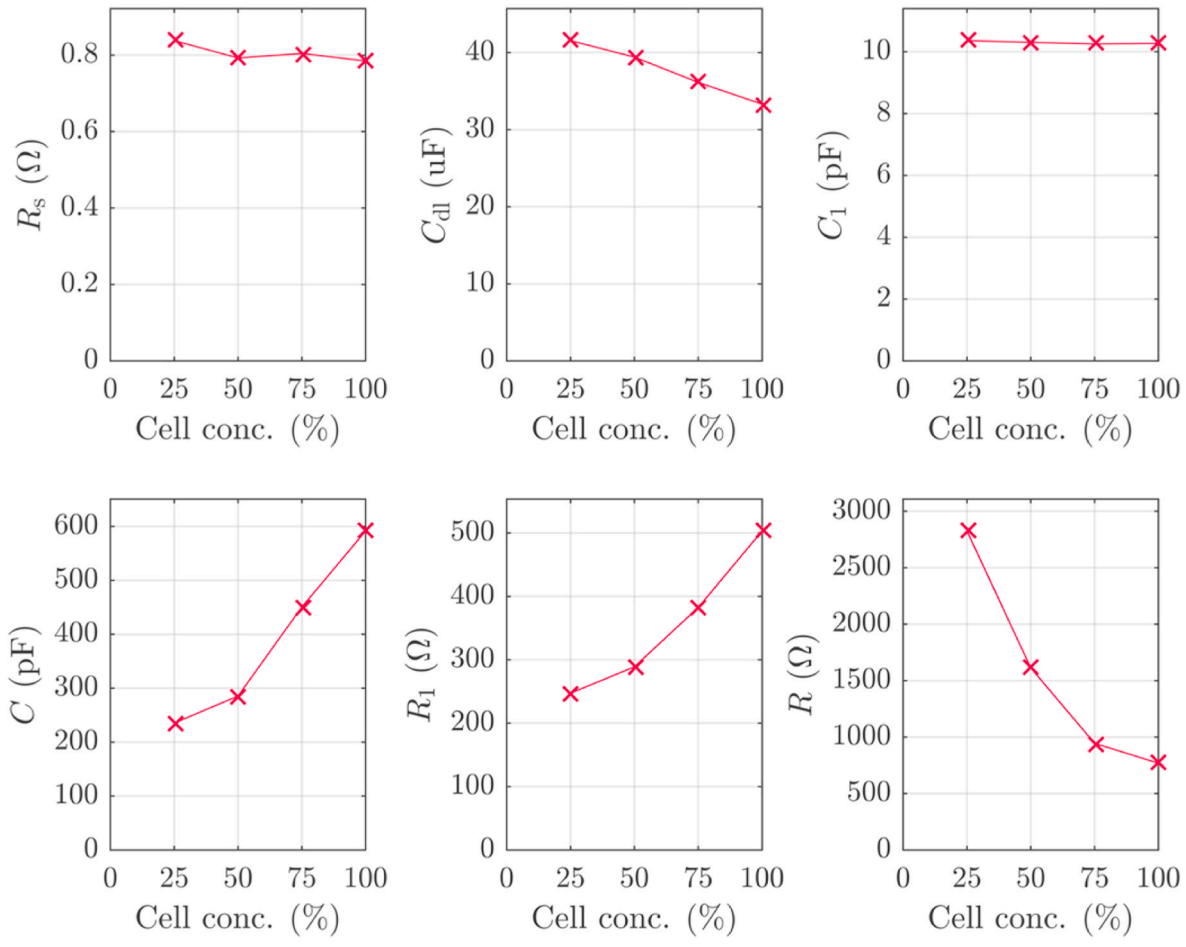

Fig. 6. The unified model electrical parameters vs. concentration of MSK8 cells in MS.

solution. It is compared with the media without cells, (e.g. the control sample), whilst the behavior of the fitted equivalent circuit representing the impedance spectrum of our system is shown be the dotted lines.

In order to combine the three ranges together, factoring was required to match the differences in the absolute values of the impedance due to geometrical differences of the MUT, since different probes were used. The middle and high frequency results were factored to match the low frequency (parallel plate) impedance. It means that the impedance that is presented in Fig. 4, is the effective parallel plate impedance over the whole frequency range. Once the effects of the probes were removed and the impedance of the middle and high frequency was factored in, the impedance and phase of the parallel plate apparatus (Fig. 3) in the complete frequency range was obtained.

The data shown in Fig. 4 suggests that the equivalent circuit model adequately fits the measured data over the whole frequency range. The agreement between the measured data and the fitting spectra indicates that the equivalent circuits provided a feasible, if not unique, model to describe the impedance characteristics within the whole frequency range.

Fig. 5 shows the simulated behavior of the equivalent circuit with component values obtained from the low frequency and high frequency data. The middle frequency data were used to confirm that the behavior of the suspension in that range matches the real data obtained. In this wide frequency range, three dispersions are observed. The first is the β dispersion at low frequencies. The second one, at around 1 MHz, is due to the cells since it does not appear when the cells are not present. The third one, at approximately 2 GHz, is due to the polarization of water molecules. Based on the literature (Asami, 2002b; Markx and Davey, 1999) another dispersion exists (α dispersion) at very low frequencies, which does not appear here since it is outside the investigated frequency range.

Another important observation from Fig. 5 is that during the purely resistive phase (approximately 100 Hz-10 kHz), the magnitude of the impedance increases with increasing cell concentration. This can be explained by the fact that the cells are less conductive compared to the medium (Wang et al., 2017), and as the concentration increases, more cells cover the electrode's surface, increasing the resistance of the solution. At higher frequencies, where the impedance is governed by the polarization of water molecules, variations in cell concentration have minor effect on the impedance and phase of the MUT.

4.2. The effect of cell concentration

In order to further investigate the effect of the cells on the impedance of the MUT, the results were normalized by the behavior of the solution without the cells using the modelled data. Fig. 6 shows the normalized behavior of the MUT, clearly indicating the effects of the cells on the impedance.

During the resistive phase (approximately 100 Hz-10 kHz), as the cell concentration increases, the impedance of the MUT also increases. Additionally, within the range of 100–400 kHz, the magnitude of the capacitance due to the cells increases with increasing cell concentration. This can be concurred by the literature (Asami, 2002b) as more cells can be assumed to be organized in parallel.

Fig. 6 shows the relationships between the values of the parameters of the equivalent circuit and the concentration of the cells. R_{ct} and the CPE parameters were not plotted because they are relatively constant for all concentrations.

R_s can be assumed to be relatively constant. R_1 increases with increasing cell concentration, whilst R decreases with increasing cell concentration. Also note that R and R_1 are much larger than R_s. Therefore, both R_1 and R determine the impedance at the intermediate range. Both R and R_1 are assumed to be responsible for the changes in the impedance as function of the cells' concentration during the resistive state of the MUT. R_1 changes by a factor of ~2 from the 25%–100% concentrations. This is shown in Fig. 6 where the measured impedance values in the frequency range of 100 Hz-100 kHz change by a factor of ~2 from 25% to 100% cell concentrations.

C_1, which represents the polarization of water molecules, is unaffected by the concentration of the cells. The double layer capacitance, C_{dl}, decreases as the cell concentration increases. This means that the cell has some effect on the electrolyte in the vicinity, within the Debye length, of the electrodes. One possible explanation is that it is attributed to the attachment of the cells to the electrode's surface. This effect can be due to the decrease of the effective electrode surface area by the cells' adherence or due to the effect of organic molecules secreted by the cells. More interestingly, the magnitude of the capacitance due to the cells (C), as well as the resistance (R), change significantly with cell concentration. C increases and R decreases with increasing cell concentration. C increases by a factor of ~3 whilst R decreases by a similar value. Theoretically the values of the C and R should asymptotically tend to zero, assuming that the effect of the ions or other polar molecules in the solution do not affect the C and R values. In reality, the ions and polar molecules do play a role on the C and R values hence they do not tend to zero. However, due to fact that the cell concentrations tested, especially at the lower range, were not very dense, the exact behavior of the values is yet to be fully described. The time constant RC remains, within the experimental error, constant. This means that both refer to the time constant that is related to the same loss mechanism, which is due to the presence of the cells in the electrolyte.

The cells membrane (Figure S4.2a) is made up of insulating lipid bilayer sandwiched between two conductive protein layers. Under alternating electrical excitation, the cell membrane behaves like capacitors, which can be modelled as a capacitor in series with a resistor that can also be used to model the resistive nuclear parts of the cell (Figure S4.2b).

The observed increase in capacitance with increasing cell concentration can be attributed to the multiple cells present in the suspension in a mostly parallel configuration. In such a configuration, the effective capacitance is the addition of the individual capacitances. However, the resistance of the inside of the cells shows a decrease with increasing cell concentration because the total resistance decreases when multiple resistances are arranged in parallel. These effects and the build-up of charge at cell membranes have been reported in the literature as the Maxwell–Garnett effect (Garnett, 1906, 1904; Markel, 2016).

5. Conclusions

A simple equivalent circuit model for cell suspensions has been presented that can be used in an ultra-wide frequency range, from 4 Hz to 20 GHz. The model is based on the classical Randles model in series with a circuit model based on the Debye relationships of relative permittivity, which takes into account the various relaxation processes in the cell/electrolyte system. The model has been tested in cell suspensions of various concentrations of plant cells (MSK8) in MS media. The data was collected using three different experimental setups in order to cover the whole range. The relationships between the values of the circuit's lumped components and cell concentrations were investigated yielding clear correlations between cell membrane capacitances and adhesion of cells on the electrodes. More specifically, it was found that the cell capacitance (C) increased within the range of 200–600 pF, whilst cell resistance (R) decreased within the range of approximately 0.8–3 kΩ with cell concentration (X–Y cells/mL) due to the multiple cells present in the suspension in a mostly parallel configuration. Additionally, the double layer capacitance, C_{dl}, decreased as the cell concentration increased, possibly due to the attachment of the cells to the electrode's surface.

This model that reported here can span throughout such a wide frequency range and incorporate both electrode interfacial effects at low frequencies and also molecule and cell polarization effects at higher frequencies. This method yields information about the electrolyte, the cells, the interaction between the cells and the electrolyte thus it can be

used for monitoring and screening of cells in electrolyte environment. The proposed model can therefore be used for future biosensor design, simulation and integration with very large scale integrated (VLSI) circuits with or without RF components using conventional computer aided design tools. However, in order to fully validate the proposed unified model more work is needed, especially on a wider variety of plant cell types, with or without modifications (i.e. using nanoparticles for example) with different cell concentrations, especially in the lower concentration range, whilst investigating multiple buffer electrolytes.

CRediT authorship contribution statement

Kian Kadan-Jamal: Investigation, Methodology, Writing - original draft, Writing - review & editing, Formal analysis. **Marios Sophocleous:** Methodology, Writing - original draft, Writing - review & editing, Formal analysis, Conceptualization. **Aakash Jog:** Methodology, Writing - review & editing, Visualization, Software, Data curation, Formal analysis. **Dayananda Desagani:** Methodology, Investigation. **Orian Teig-Sussholz:** Methodology, Investigation. **Julius Georgiou:** Supervision. **Adi Avni:** Writing - review & editing, Methodology, Supervision, Resources. **Yosi Shacham-Diamand:** Writing - original draft, Writing - review & editing, Methodology, Supervision, Resources, Investigation, Validation, Formal analysis, Conceptualization.

Declaration of competing interest

The authors declare that they have no known competing financial interests or personal relationships that could have appeared to influence the work reported in this paper.

Acknowledgements

The research was partially funded by the Ministry of Science and Technology, Israel, Grant # 3–14345 titled “Single cell Sensor”. It was also partially supported by the Israel Science Foundation (Grant no. 1616/17). We would also like to acknowledge the Boris Mints Institute for Strategic Policy Solutions to Global Challenges, the Department of Public Policy and the Manna Centre for Food Security, Tel Aviv University for their generous support under the program “Plant based heat stress whole-cell-biosensor” (Grant no. 590351) 2017.

The authors gratefully acknowledge the support of Prof. Eran Socher and the lab manager Avigdor Drucker from the High Frequency Integrated Circuits Lab, School of Electrical Engineering - Physical Electronics at Tel Aviv University for the opportunity to do the high frequency measurements in his Lab.

Special Thanks goes to Dr. Rachel Shmuel, and her team from the workshop in the faculty of Engineering at Tel Aviv University, for their help and meeting the deadlines.

Appendix A. Supplementary data

Supplementary data to this article can be found online at https://doi.org/10.1016/j.bios.2020.112485.

References

Andreescu, S., Sadik, O.A., McGee, D.W., Suye, S.I., 2004. Anal. Chem. 76, 2321–2330. https://doi.org/10.1021/ac035436m.
Asami, K., 2002a. J. Non-Cryst. Solids 305, 268–277. https://doi.org/10.1016/S0022-3093(02)01110-9.
Asami, K., 2002b. Prog. Polym. Sci. 27, 1617–1659. https://doi.org/10.1016/S0079-6700(02)00015-1.
Asami, K., 2014. Colloids Surf. B Biointerfaces 119, 1–5. https://doi.org/10.1016/j.colsurfb.2014.04.014.
Asami, K., Yamaguchi, T., 1992. Biophys. J. 63, 1493–1499. https://doi.org/10.1016/S0006-3495(92)81734-4.
Asami, K., Hanai, T., Koizumi, N., 1976. J. Membr. Biol. 28, 169–180. https://doi.org/10.1007/BF01869695.
Asami, K., Hanai, T., Koizumi, N., 1980. Jpn. J. Appl. Phys. 19, 359–365. https://doi.org/10.1143/JJAP.19.359.
Asami, K., Takahashi, Y., Takashima, S., 1989. Dielectric Properties of Mouse Lymphocytes and Erythrocytes.
Asami, K., Yonezawa, T., Wakamatsu, H., N, K., 1996. Bioelectrochem. Bioenerg. 40, 141–145.
Bard, A., Faulkner, L., 2001. Electrochemical Methods: Fundamentals and Applications, 2nd. John Wiley & Sons, USA.
Barsoukov, Evgenij, J, .R.M., 2005. Impedance spectroscopy theory, experiment, and applications. In: Journal of Applied Electrochemistry, second ed. John Wiley & Sons, Inc. https://doi.org/10.1016/j.snb.2007.02.003.
Bera, T.K., Nagaraju, J., Lubineau, G., 2016. J. Vis. 19, 691–713. https://doi.org/10.1007/s12650-016-0351-0.
Beving, H., Eriksson, L.E.G., Davey, C.L., Kell, D.B., 1994. Eur. Biophys. J. 23, 207–215.
Bordi, F., Cametti, C., Rosi, A., Calcabrini, A., 1993. Biochim. Biophys. Acta 1153, 77–88.
Carstensen, E.L., 1967. Biophys. J. 7, 493–503. https://doi.org/10.1016/S0006-3495(67)86600-1.
Carvell, J.P., Dowd, J.E., 2006. Cytotechnology 50, 35–48. https://doi.org/10.1007/s10616-005-3974-x.
Chen, H., Heng, C.K., Puiu, P.D., Zhou, X.D., Lee, A.C., Lim, T.M., Tan, S.N., 2005. Anal. Chim. Acta 554, 52–59. https://doi.org/10.1016/j.aca.2005.08.086.
Cole, K.S., Cole, R.H., 1942. J. Chem. Phys. 10, 98–105. https://doi.org/10.1063/1.1723677.
Corona-Lopez, D.D.J., Sommer, S., Rolfe, S.A., Podd, F., Grieve, B.D., 2019. Plant Methods 15, 1–15. https://doi.org/10.1186/s13007-019-0438-4.
Davidson, D.W., Cole, R.H., 1950. J. Chem. Phys. 18, 1417. https://doi.org/10.1063/1.1747496.
Debye, P., 1929. Polar Molecules. Chemical Catalogue Company, New York.
Garnett, J.C.M., 1904. Phil. Trans. A 203, 385.
Garnett, J.C.M., 1906. Phil. Trans. Roy. Soc. Lond.
Grimnes, S., Martinsen, Ø.G., Grimnes, S., Martinsen, Ø.G., 2015. Chapter 3 – Dielectrics, Bioimpedance and Bioelectricity Basics. https://doi.org/10.1016/B978-0-12-411470-8.00003-9.
Guan, J., Miao, Y., Zhang, Q., 2004. 97, 219–226.
Guo, M., Chen, J., Yun, X., Chen, K., Nie, L., Yao, S., 2006. Biochim. Biophys. Acta Gen. Subj. 1760, 432–439. https://doi.org/10.1016/j.bbagen.2005.11.011.
Havriliak, S., Havriliak, S.J., 1996. Polymer 37, 4107–4110. https://doi.org/10.1016/0032-3861(96)00274-1.
Havriliak, S., Negami, S., 1966. J. Polym. Sci. Part C Polym. Symp. 14, 99–117. https://doi.org/10.1002/polc.5070140111.
Herman, P., 1991. Schwan and Shiro Takashim. Chem. Res. 69, 300.
Höber, R., 1910. Pflüger's Arch. für die Gesammte Physiol. des Menschen und der Tiere 133, 237–253. https://doi.org/10.1007/BF01680330.
Irimajiri, A., Doida, Y., Hanai, T., Inouye, A., 1978. J. Membr. Biol. 38, 209–232. https://doi.org/10.1007/BF01871923.
Jenin, P.C., Schwan, H.P., 1980. Biophys. J. 30, 285–293. https://doi.org/10.1016/S0006-3495(80)85094-6.
Khaled, D. El, Castellano, N.N., Gázquez, J.A., Perea-Moreno, A.J., Manzano-Agugliaro, F., 2016. Materials (Basel), vol. 9, pp. 1–26. https://doi.org/10.3390/ma9050310.
Koornneef, M., Hanhart, C.J., Martinelli, L., 1987. Theor. Appl. Genet. 74, 633–641. https://doi.org/10.1007/BF00288863.
Lei, K.F., Wu, M.H., Hsu, C.W., Chen, Y.D., 2014. Biosens. Bioelectron. 51, 16–21. https://doi.org/10.1016/j.bios.2013.07.031.
Liu, Q., Yu, J., Xiao, L., Tang, J.C.O., Zhang, Y., Wang, P., Yang, M., 2009. Biosens. Bioelectron. 24, 1305–1310. https://doi.org/10.1016/j.bios.2008.07.044.
Markel, V.A., 2016. J. Opt. Soc. Am. A 33, 1244. https://doi.org/10.1364/josaa.33.001244.
Markx, G.H., Davey, C.L., 1999. 25, 161–171.
Murasnige, T., Skoog, F., n.d A Revised Medium for Rapid Growth and Bio Agsays with Tohaoco Tissue Cultures.
Nelson, S.O., 1981. Cereal Chemestry 58, 487–492.
Nelson, S.O., 1991. IEEE Trans. Electr. Insul. 26, 845–869. https://doi.org/10.1109/14.99097.
Orazem, M.E., Tribollet, B., 2017. Electrochemical Impedance Spectroscopy. John Wiley & Sons.
Pethig, R., Kell, D.B., 1987. Phys. Med. Biol. 32, 933–970. https://doi.org/10.1088/0031-9155/32/8/001.
Randles, J.E.B., 1947. Faraday Discuss.
Ribaut, C., Reybier, K., Reynes, O., Launay, J., Valentin, A., Fabre, P.L., Nepveu, F., 2009. Biosens. Bioelectron. 24, 2721–2725. https://doi.org/10.1016/j.bios.2008.12.018.
Schwan, H.P., Li, K., 1953. Proc. IRE 41, 1735–1740. https://doi.org/10.1109/JRPROC.1953.274358.
Skierucha, W., Wilczek, A., Szypłowska, A., 2012. Int. Agrophys. 26, 187–197. https://doi.org/10.2478/v10247-012-0027-5.
Surowiect, A., Stuchly, S.S., IzaguirreS, C., 1986. Phys. Med. Biol 31, 43–53.
Touw, F. Van Der, Briedé, J.W.H., Mandel, M., 1973. Biopolymers 12, 111–119. https://doi.org/10.1002/bip.1973.360120110.
Trabelsi, S., Nelson, S.O., 2003. Conf. Rec. - IEEE Instrum. Meas. Technol. Conf. 1, 518–523. https://doi.org/10.1109/imtc.2003.1208212.
Trabelsi, S., Nelson, S.O., 2016. IEEE Instrum. Meas. Mag. 19, 36–41. https://doi.org/10.1109/MIM.2016.7384959.
Wang, K., Zhao, Y., Chen, D., Fan, B., Lu, Y., Chen, L., Long, R., Wang, J., Chen, J., 2017. Sci. Data 4, 1–8. https://doi.org/10.1038/sdata.2017.15.